Stratospheric age spectra derived from observations of water vapor and methane

David G. Johnson, Kenneth W. Jucks, Wesley A. Traub, and Kelly V. Chance
Smithsonian Astrophysical Observatory, Cambridge, Massachusetts

Geoffrey C. Toon
Jet Propulsion Laboratory, Pasadena, California

James M. Russell III and M. Patrick McCormick
Department of Physics, Hampton University, Hampton, Virginia

Abstract

The stratospheric age spectrum is useful both as a diagnostic for testing models of stratospheric transport and as a tool for calculating the response of the stratosphere to changes in tropospheric composition. Although the age spectrum of an individual air parcel is not an observable quantity, it is possible to estimate a zonal mean age spectrum from long-term observations of a conserved tracer with sufficient temporal variability. We have constructed a conserved tracer by combining satellite and balloon-borne observations of water vapor and methane from 1986 to 1998. After discussing the possible roles of tropical sea surface temperatures and the quasi-biennial oscillation in determining stratospheric humidity, we use the observations to estimate the zonal mean age spectrum in the tropics and northern midlatitudes. The estimated age spectrum peaks at progressively greater lag times as the altitude increases above the tropopause, in agreement with model calculations. The mean age of air calculated from the derived age spectrum in the lower stratosphere is in good agreement with ages calculated from measurements of SF_6, but the satellite record is still too short to calculate reliable ages from the age spectrum in the middle and upper stratosphere.

1. Introduction

The stratospheric age spectrum, or probability distribution for the ages defined by an ensemble of trajectories [*Hall and Plumb,* 1994, and references therein], provides a description of the transport history of an individual air parcel. We assume here that air enters the stratosphere in the tropics [e.g., *Holton et al.,* 1995], and we define age to be the time since crossing the tropical tropopause. Let $V(\boldsymbol{x}, t)$ represent the volume mixing ratio (vmr) of a conserved tracer at time t and location $\boldsymbol{x}$. If the tropical tropopause is located at $\boldsymbol{x}_0$, then

$$V(\boldsymbol{x}, t) = \int_0^\infty d\tau\, G(\boldsymbol{x}, t, \tau)\, V(\boldsymbol{x}_0, t - \tau), \qquad (1)$$

where G is the age spectrum for the parcel at location $\boldsymbol{x}$ and time t as a function of lag time τ and $\int_0^\infty d\tau\, G(\boldsymbol{x}, t, \tau) = 1$. Following *Hall and Plumb* [1994], we define the mean age $\Gamma(\boldsymbol{x}, t)$ as follows:

$$\Gamma(\boldsymbol{x}, t) = \int_0^\infty d\tau\, \tau G(\boldsymbol{x}, t, \tau). \qquad (2)$$

If V is increasing linearly with time, such that $V(\boldsymbol{x}_0, t) = mt + b$, it follows from (1) and (2) that $V(\boldsymbol{x}, t) = V(\boldsymbol{x}_0, t) - m\Gamma(\boldsymbol{x}, t)$. The mean age for an air parcel can thus be determined from the measured mixing ratio of a linearly increasing tracer if the trend at the tropical tropopause is known. The age spectrum for a single air parcel cannot be observed since only the mean composition of a limited number of tracers can be measured, nor can changes in the composition of the parcel over time be determined, since the identities of individual parcels are lost through mixing. Because of these limitations, mean age has seen more practical use than the age spectrum, although the age spectrum provides a less ambiguous description of the transport history.

In the following sections we demonstrate that $G(\boldsymbol{x}, t, \tau)$ can be estimated from measurements of $V(\boldsymbol{x}, t)$ and $V(\boldsymbol{x}_0, t)$ if several conditions are met. We require that G can be approximated by the zonal mean age spectrum $\bar{G}$, that $\bar{G}$ be a function of $\boldsymbol{x}$ and τ only, and that the power spectrum of $V(\boldsymbol{x}, t)$ be sufficiently rich, as explained in section 2.. We show that a suitable conserved tracer can be derived from measurements of the water vapor (H_2O) vmr by correcting for the effects of methane (CH_4) oxidation. After constructing a 12-year record of corrected H_2O by combining measurements made by the Stratospheric Aerosol and Gas Experiment II (SAGE II) and the Halogen Occultation Experiment (HALOE) as described in section 4., we show that the H_2O vmr has sufficient temporal variability to serve as V. Finally, after discussing possible sources of variability in section 5., we use the corrected H_2O data to estimate G at selected altitudes in the tropics and middle latitudes.

2. Zonal Mean Age Spectrum

We begin by assuming that $V(\boldsymbol{x}_0, t)$ can be approximated by the zonal mean, $\bar{V}(\boldsymbol{x}_0, t)$. This approximation is justified since the zonal mixing time in the tropics is short compared to the vertical and meridional advection timescales. After making this substitution we calculate the zonal mean of both sides of (1) and derive the equivalent expression relating $\bar{V}(\boldsymbol{x}, t)$, $\bar{V}(\boldsymbol{x}_0, t)$, and $\bar{G}$. The advantage of taking the zonal mean is that the time evolution of $\bar{V}(\boldsymbol{x}, t)$ can be measured, while the evolution of $V(\boldsymbol{x}, t)$ cannot, since the identities of individual parcels are not preserved by mixing. After making the additional assumption that $\bar{G}$ does not depend on t, we derive the equivalent zonal mean expression:

$$\bar{V}(\boldsymbol{x}, t) = \int_0^\infty d\tau\, \bar{G}(\boldsymbol{x}, \tau)\, \bar{V}(\boldsymbol{x}_0, t - \tau). \qquad (3)$$

According to the convolution theorem, (3) is equivalent to

$$\bar{v}(\boldsymbol{x}, \omega) = \bar{g}(\boldsymbol{x}, \omega)\bar{v}(\boldsymbol{x}_0, \omega), \qquad (4)$$

where $\bar{v}$ and $\bar{g}$ are the Fourier transforms of $\bar{V}$ and $\bar{G}$, respectively.

In principle, we can calculate $\bar{G}(\boldsymbol{x}, \tau)$ by taking the inverse transform of $\bar{v}(\boldsymbol{x}, \omega)/\bar{v}(\boldsymbol{x}_0, \omega)$. Doing so in practice requires that we be able to measure $\bar{v}$ with sufficient precision (the calculation is unaffected by systematic errors which do not depend on $\boldsymbol{x}$ or t) and that $\bar{v}(\boldsymbol{x}_0, \omega)$ be nonzero at all frequencies where $\bar{g}$ is significant. We show an example of the procedure in Figure 1. We convolved a test signal (the NINO4 index, defined as the average sea surface temperatures in the region bounded by 5°N–5°S and 160°E–150°W, retrieved from the Climate Prediction Center at http://nic.fb4.noaa.gov/data/cddb/; we used monthly average data, available from 1950 through the present) with a sample age spectrum to produce $\bar{V}(\boldsymbol{x}, t)$. We then calculated the Fourier transforms of $\bar{V}(\boldsymbol{x}, t)$ and $\bar{V}(\boldsymbol{x}_0, t)$ (the original test signal) and calculated the inverse transform of the ratio to estimate $\bar{G}$. The best results are obtained by apodizing the data with a Hann window before the forward transform (to minimize ringing) and then applying a Weiner filter before the reverse transform [*Press et al.*, 1992]. We estimated the age spectrum using 12-year (the length of the data record analyzed in section 6.) and 39-year data records. The longer record produces a better estimate of the age spectrum because it

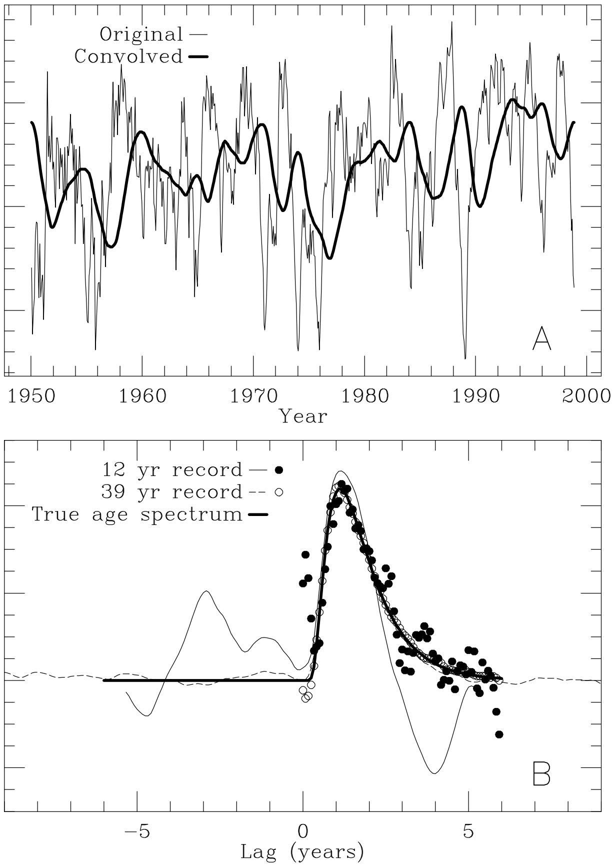

Figure 1. (a,b) Example of age spectrum recovery. A test signal (Figure 1a, light curve) is convolved with a sample age spectrum (Figure 1b, heavy curve) to produce a smoothed and time-shifted signal (Figure 1a, heavy curve). Fourier deconvolution was used to recover the age spectrum from the full data set (Figure 1b, dashed curve) and from a subset of the data (Figure 1b, light curve) covering the period 1986.0–1997.8. Also shown are results of singular-value decomposition (SVD) deconvolution of the full data set (Figure 1b, open circles) and of the subset (Figure 1b, solid circles).

provides a better estimate of the low-frequency power in $\bar{G}$.

The Fourier deconvolution method requires that the tracer concentration be evenly sampled in time in both the source and target regions, a condition that is hard to meet in practice for time periods covering a decade or more. While the success of any deconvolution method depends on having a high-quality data record in the source region, the requirement of even sampling in both the source and target regions is imposed by the Fourier analysis method and is not intrinsic to the deconvolution problem.

As an alternative, we have developed a deconvolution method which is equivalent to solving a set of linear equations. We first rewrite (1) as the set of $n+1$ discrete sums:

$$\bar{V}(\boldsymbol{x}, t_i) = \sum_{j=0}^{m} \bar{G}(\boldsymbol{x}, \tau_j) \bar{V}(\boldsymbol{x}_0, t_i - \tau_j), \qquad (5)$$

where $t_i = t_0 + i\delta t$, $\tau_j = j\delta t$, $\bar{V}(\boldsymbol{x}, t_i)$ is the average tracer concentration over the interval $t_i - \delta t/2 < t_i < t_i + \delta t/2$, $0 \leq i \leq n$, and m is chosen such that $\bar{G}(\boldsymbol{x}, \tau_{j>m}) \approx 0$. We can solve (5) for $\bar{G}$ using, for example, singular-value decomposition (SVD) [*Press et al.*, 1992], provided $n > m$. An example of the SVD deconvolution is shown in Figure 1b. The calculated age spectra have been smoothed with a Savitzky-Golay filter [*Press et al.*, 1992] before plotting. For the full data record the results are comparable to the results from Fourier deconvolution, while for the data subset the SVD method does the best job of recovering the original age spectrum.

Estimating the age spectrum requires a data record which is at least as long as the full width of the age spectrum, where the width is defined as the range in τ for which $\bar{G}$ exceeds some fraction α of the peak value. For $\alpha = 0.25$ we need a continuous set of measurements of a conserved tracer covering more than 5 years to estimate the age spectrum outside the tropical lower stratosphere [*Hall and Waugh,* 1997]. Water vapor is a promising tracer (although not strictly conserved because of the oxidation of methane), since nearly continuous global measurements have been available in the stratosphere since 1986 [*McCormick et al.,* 1993].

3. Water Vapor as a Conserved Tracer

The H_2O vmr of air entering the stratosphere follows a strong annual cycle [*Mote et al.,* 1998, *McCormick et al.,* 1993], with a peak-to-peak amplitude of 2.2 parts per million (ppm) by volume superposed on a mean value of 3.6 ppm. Oxidation of methane (CH_4) as the air rises produces 1.6–2.0 molecules of H_2O for each molecule of CH_4 destroyed [*Remsberg et al.,* 1996, *Abbas et al.,* 1996], gradually increasing the abundance of H_2O by several ppm.

The effect of methane oxidation can be removed by considering the quantity $Q = [\mathrm{H_2O}] + 2[\mathrm{CH_4}]$, where $[x]$ signifies the vmr of x. Because Q is approximately conserved in the stratosphere [*Abbas et al.,* 1996, *Nedoluha et al.,* 1998], we can estimate initial [H_2O] from Q by subtracting twice the initial [CH_4] (approximately 1.71 ppm.) As is the case for mean age, the estimated initial [H_2O] (hereinafter called entry level H_2O) is actually an average over the ensemble of trajectories across the tropopause which make up an air parcel at a particular time and place.

Estimation of entry level [H_2O] is complicated by the fact that tropospheric [CH_4] is not constant [*Dlugokencky et al.,* 1994]. A proper calculation of entry level [H_2O] would require first estimating the initial [CH_4] by convolving the record of tropospheric [CH_4] with the age spectrum. We choose instead to use a constant value of 1.71 ppm for initial [CH_4] and substitute $Q - 3.42$ ppm for V (in (3) and (5), for example). While this will cause a small error in our estimate of entry level [H_2O] (discussed in section 5.1.), it does not affect the calculation of the age spectrum.

Water can be destroyed through photolysis and reaction with O(^1D), although in the stratosphere the products quickly recombine to form water. Actual loss of H_2O requires shifting H atoms to another reservoir, such as HCl, HF, HNO_3, H, or H_2. At altitudes below 35 km, H_2 is the only significant hydrogen reservoir besides Q, and previous analyses have shown that [H_2] is nearly constant below 35 km [*Abbas et al.,* 1996]. We therefore assume that Q is conserved below 35 km.

Several recent analyses have reported long-term increases in stratospheric H_2O superposed on the annual cycle, with estimates ranging from 15 to 70 parts per billion (ppb)/yr [*Oltmans and Hofmann,* 1995, *Nedoluha et al.,* 1998, *Evans et al.,* 1998]. The trend is generally in excess of that expected from the 10 ppb/yr increase in CH_4 [*Dlugokencky et al.,* 1994], leading to the conclusion that there has been an increase in the amount of H_2O entering the stratosphere at the tropical tropopause, possibly as a result of climate change [*Oltmans and Hofmann,* 1995, *Nedoluha et al.,* 1998, *Evans et al.,* 1998]. As we describe in section 5., H_2O shows significant variations in addition to the long-term increase and annual cycle, which increase its usefulness as a tracer of motion.

4. Data Analysis

We construct global estimates of entry level H_2O covering 12 years (1986–1997) by combining measurements made by HALOE (November 1991 to November 1997) and SAGE II (January 1986 to May 1991). We use midlatitude data from two balloon experiments, the Jet Propulsion Laboratory Mark IV (MkIV) interferometer and the Smithsonian Astrophysical Observatory Far-infrared Spectrometer 2 (FIRS-2), to correct for systematic differences between HALOE and SAGE II. The H_2O measurements from all four instruments are corrected separately for CH_4 oxidation, and then systematic differences between instruments are removed. The results presented here include data from two latitude bands, 25°–35°N (the latitude of most of the balloon flights) and 15°S–15°N.

The MkIV is a midinfrared Fourier transform spectrometer operated in solar-occultation mode from balloon and aircraft platforms and from the ground [*Toon,* 1991, *Toon et al.,* 1992]. The data analyzed here were obtained during sunrise and sunset observations on eight balloon flights between September 1990 and May 1997. Mixing ratio profiles were obtained at latitudes near 35°N, with the exception of the last flight (68°N). Of the many species observed by the MkIV, only measurements of H_2O, CH_4, nitrous oxide (N_2O), and potential temperature (θ) are considered here. Profiles are retrieved onto a 1-km altitude grid and have an estimated vertical resolution of 2-3 km. The entry level H_2O is approximated by $\hat{X} = X - 2(B_0 - B)$, where $\hat{X}$ is the entry level H_2O vmr, X is the observed vmr, B is the observed CH_4 vmr, and B_0 is the entry level CH_4 vmr (assumed to be 1.71 ppm). We then derive a relationship between CH_4, N_2O, and θ, which is used in the analysis of FIRS-2 data to estimate CH_4. The estimated systematic error in MkIV retrievals is 5% or less.

The FIRS-2 is a far-infrared and midinfrared Fourier transform spectrometer which observes the atmosphere in thermal emission [*Johnson et al.,* 1995]. Profiles are retrieved onto a 1-km altitude grid and have a vertical resolution of 3-4 km. The data analyzed here were obtained during six balloon flights between September 1989 and April 1997, and with the exception of the 1997 flight (Alaska, at 68°N) all observations were made between 25° and 35°N. For the present analysis we use only FIRS-2 measurements of H_2O, N_2O, and θ, although many other species are observed. We estimate B using FIRS-2 measurements of N_2O and θ and the CH_4 relation derived from MkIV data, and we then calculate $\hat{X}$ as above. The estimated systematic error in the FIRS-2 retrievals used here is 7% for H_2O and 3% for N_2O.

Table 1. Water Vapor Mixing Ratio Biases Between Instruments

Altitude, km	FIRS-2−SAGE II, ppm	MkIV−SAGE II, ppm	FIRS-2−HALOE, ppm	MkIV−HALOE, ppm
16.5	0.29±0.30	0.56±0.29	0.82±0.21	0.79±0.23
18.5	1.48±0.88	1.60±0.32	0.88±0.21	0.79±0.14
21.5	0.51±0.27	0.76±0.23	0.19±0.07	0.25±0.13
26.5	−0.06±0.19	0.24±0.34	0.16±0.07	0.38±0.11
31.5	−0.30±0.53	−0.14±0.24	0.22±0.08	0.42±0.10

Monthly zonal mean satellite data are interpolated to the date of each balloon flight, and the differences are averaged over all flights for each instrument pair. Comparisons are with zonal mean satellite data and not the single profile nearest the balloon, increasing precision in the satellite data but decreasing the geographic coincidence with the balloon data. FIRS-2, Far-infrared Spectrometer 2; SAGE II, Stratospheric Aerosol and Gas Expermient II; MkIV, Mark IV; HALOE, Halogen Occultation Experiment.

HALOE, launched on the Upper Atmosphere Research Satellite in 1991, has a gas correlation radiometer and a filter radiometer, which both operate in the solar occultation mode [*Russell et al.*, 1993]. We use level 3 data (version 18), which are interpolated onto a standard pressure grid ($\Delta \log(P) = 0.1667$). The gas correlation radiometer used for CH_4 measurements provides a vertical resolution of 4.5 km, while the filter radiometer used for H_2O provides a resolution of 2-3 km. Data were obtained from the National Aeronautics and Space Administration (NASA) Goddard Distributed Active Archive Center (DAAC) for November 1991 through November 1997 (available at http://daac.gsfc.nasa.gov/DAAC_DOCS/-gdaac_home.html). We calculate monthly zonal mean profiles for CH_4 and H_2O for the latitude bands 15°S to 15°N and 25°N to 35°N and estimate $\hat{X}$ as above. The estimated systematic errors in HALOE CH_4 and H_2O average 12% and 19%, respectively [*Harries et al.,* 1996, *Park et al.,* 1996].

SAGE II is a seven-channel solar occultation spectrometer which was launched on the Earth Radiation Budget Satellite in 1984 and continues to operate [*McCormick et al.,* 1993]. The water channel is sensitive to aerosols, and at present only data for the low-aerosol period January 1986 through May 1991 are available. Profiles are retrieved on a 1-km altitude grid. We obtained version 5.9 H_2O data from the NASA Langley DAAC (available at http://eosweb.larc.nasa.gov/) and calculated monthly zonal mean profiles as for HALOE. Any measurements for which the aerosol optical depth exceeds 1.3×10^{-4} per km (corresponding to roughly 50% of the total optical depth in the water channel [see *Rind et al.,* 1993]) were excluded to minimize systematic errors; this eliminates much of the data between 18 and 26 km. Because the systematic error due to aerosols results from uncertainties in separating the individual contributions of H_2O and aerosols to observed optical depth, and not from errors in the measurement of total optical depth, we believe that H_2O measurements below the aerosol layer are reliable provided the aerosol optical depth does not exceed the cutoff. We use the 6-year average zonal mean HALOE CH_4 for each latitude band to estimate B and calculate $\hat{X}$ as above. The estimated systematic error for SAGE II H_2O is 20%.

We compare estimates of $\hat{X}$ at selected altitudes (close to HALOE pressure levels) to detect and correct for systematic differences between instruments (Table 1 and Figure 2). We assume that the differences are due to simple offsets which depend on altitude but are constant in time. The bias at each altitude between a balloon and a satellite instrument is defined as the difference between the balloon measurement and the zonal mean satellite measurement for the month of the balloon flight, averaged over all balloon flights which overlap in time with the satellite measurements. The highly processed nature of $\hat{X}$ means that differences will be due to the combination of errors in individual retrievals and, in the case of FIRS-2 and SAGE II data, errors in estimating CH_4. The differences between instruments are generally less than the estimated systematic error, with the exception of the difference between SAGE II and balloon data inside the aerosol layer (18.5

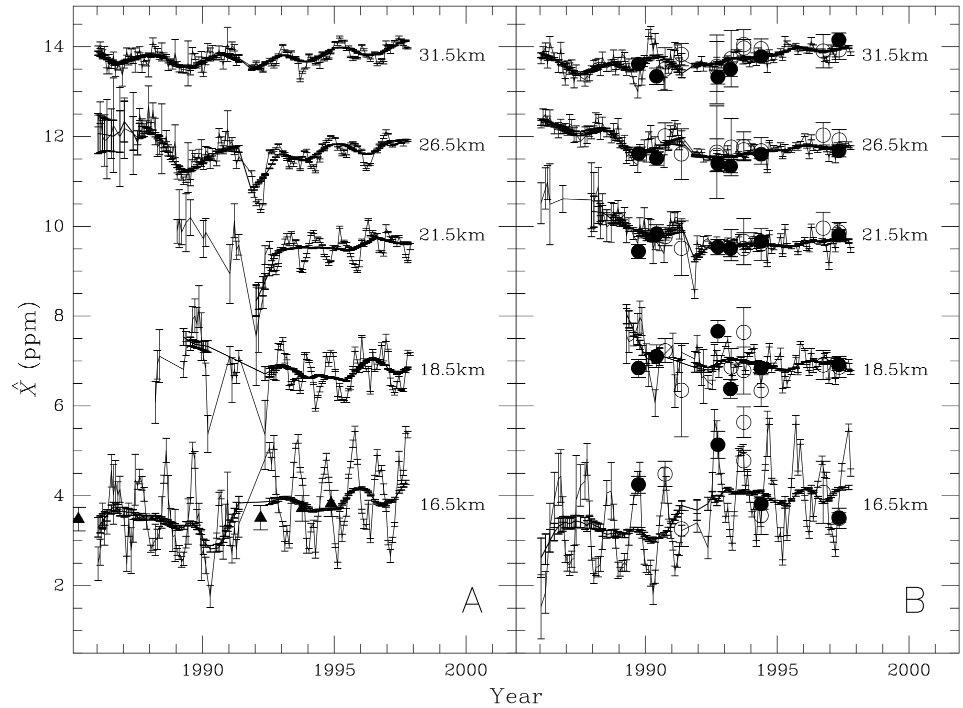

Figure 2. Combined Stratospheric Aerosol and Gas Experiment II (SAGE II) (1986–1991) and Halogen Occultation Experiment (HALOE) (1991-1997) estimates of zonal mean entry level H_2O ($\hat{X}$) in (a) the tropics and (b) the northern middle latitudes. Estimates are corrected for average offset from Far-infrared Spectrometer 2 (FIRS-2) and Mark IV (MkIV) data. FIRS-2 and MkIV data are plotted as solid and open circles, respectively; estimates of global average $\hat{X}$ from an analysis of Atmospheric Trace Molecule Spectroscopy (ATMOS) data [*Abbas et al.,* 1996] are plotted as triangles at 16.5 km (Figure 2a). Heavy curve indicates result after removing annual and semiannual cycles ($\hat{X}_s$); SAGE II and HALOE are processed separately. The data at 18.5, 21.5, 26.5, and 31.5 km have been offset by 3.0, 6.0, 8.0, and 10.0 ppm, respectively.

and 21.5 km). SAGE II and HALOE are corrected at each altitude by averaging results from the FIRS-2 and MkIV comparisons and adjusting $\hat{X}$ accordingly. The fact that the offsets derived from FIRS-2 and MkIV data are similar gives us added confidence in this procedure. We choose to correct the satellite data for the average offset from the balloon data because the balloon data have the greatest estimated accuracy, although the conclusions of this study are not affected by the choice of reference instrument.

5. Interannual Variability of $\hat{X}$

The annual cycle dominates the H_2O record up to 21.5 km in the tropics (Figure 2), obscuring more subtle long-term trends. We remove annual and semiannual cycles by defining a sliding time window around each measurement i and fitting a function $X(t)$ to the data $\hat{X}(t)$ inside the window, where

$$X(t_i+t_j) = a_1+a_2t_j+a_3\sin(2\pi t_j+a_4)+a_5\sin(4\pi t_j+a_6), \tag{6}$$

t_i is the time of measurement i in years, $t_j = j\delta t$, and the window is defined by $-N \leq j \leq N$. We use a window with a nominal width of 1 year, but the width may be larger if there is missing data within ± 0.5 year of t_i. The window is always defined to be symmetric in time about t_i. The smoothed value of $\hat{X}$ at time t_i ($\hat{X}_s(t_i)$) is given by a_1 (the result of setting t_j, a_3, and a_5 to 0 in equation (6)). A new set of coefficients a_1–a_6 is fit for t_{i+1}, and the process is repeated. SAGE II and HALOE data are smoothed separately. The results are shown in Figure 2.

5.1. Long-Term Trends

Two recent studies of HALOE data [*Nedoluha et al.,* 1998, *Evans et al.,* 1998] have concluded that $\hat{X}$ is increasing at a rate of around 70 ppb/yr. The observed rate of increase depends on altitude and latitude, which may indicate that $\hat{X}$ is changing in a nonlinear fashion. Although we have not performed a global analysis, we use the corrected SAGE II data set to extend the trend analysis by an additional 6 years in the tropics and northern middle latitudes. We then compare our results with the results of other studies as a test of our analysis. Significant differences between trends derived from the combined data set and other published results would be a cause for concern.

We find that while the HALOE measurements show increasing $\hat{X}$ after 1992.0 at all altitudes and latitudes considered in this study, the SAGE II data show constant or decreasing $\hat{X}$ before 1992.0 (see $\hat{X}_s$ in Figure 2). We have considered the possibility that the different trends seen by HALOE and SAGE II are due to a difference in the instruments. While the balloon data cover a sufficient time period to confirm the midlatitude trend seen by HALOE (Figure 2b), there is not enough balloon data to confirm the SAGE II trend.

Estimates of global mean $\hat{X}$ extending back to 1985 have been derived from data obtained by Atmospheric Trace Molecular Spectroscopy (ATMOS) [*Abbas et al.,* 1996], shown in Figure 2a. Although the time coverage is sparse (data were obtained during space shuttle flights in 1985, 1992, 1993, and 1994), we believe that the excellent agreement between ATMOS and the corrected SAGE II and HALOE data outside the aerosol layer confirms the trend seen in the SAGE II data set.

We estimate the long-term trend in tropical $\hat{X}$ by fitting a line to $\hat{X}_s$ at each altitude. The mean trend in tropical $\hat{X}$ from 1986 to 1997 ranges from 60 to 47 ppb/yr between 16.5 and 31.5 km. The midlatitude trends are similar. This is somewhat smaller than the estimates of around 70 ppb/yr based on HALOE data alone [*Nedoluha et al.,* 1998, *Evans et al.,* 1998], since the SAGE II data do not show the same increasing trend. A recent study of midlatitude data covering a longer time period, 1981–1994, concluded that H_2O was increasing by 30 and 14 ppb/yr at 16 and 26 km, respectively [*Oltmans and Hofmann,* 1995], an even smaller trend than that which we find in the present study.

The disagreement between the different trend studies may be due to the different time periods considered. We tested this hypothesis by performing a least squares fit to the function $H(t)$, where H is a crude approximation to the 16.5-km tropical signal shown in Figure 2. We use $H(t < 1990.0) = 3.5$ ppm and $H(t \geq 1990) = 4.0$ ppm. We find that the trends for 1986–1997 and 1981–1994 are 60 and 40 ppb/yr, respectively, roughly consistent with both the present study and the midlatitude results below 20 km.

We have ignored the trend in tropospheric CH_4 in the present analysis, assuming that $B_0 = 1.71$ ppm and applying HALOE CH_4 (1991–1997) to the analysis of older SAGE II data (1986–1991). For the range of CH_4 considered here, neglecting the trend in CH_4 (including the effect of using average HALOE CH_4 for the SAGE II time period) results in an error of less than 16 ppb in the estimate of $\hat{X}$. We have not considered the possibility of a trend in molecular hydrogen, which is not likely to contribute significantly to the trend in H_2O within the range of altitudes analyzed here because the abundance is too small [*Nedoluha et al.,* 1998].

5.2. Influence of the Quasi-biennial Oscillation and Sea Surface Temperature

Removing the annual cycle reveals several features in the tropical data at 16.5 km (Figure 2). SAGE II data show a slight decline from 1986 to 1990, followed by a dip and sharp rise. HALOE data show a gradual increase from 1992 to 1997, superimposed on an oscillation with a period of roughly 30 months. The oscillation fades with altitude up to 21.5 km but becomes prominent in both the SAGE and HALOE data above 26.5 km; the interannual variability near 27 km in HALOE measurements of Q has been noted before [*Randel et al.,* 1998].

The 30-month period suggests that $\hat{X}$ may be influenced by the quasi-biennial oscillation (QBO) in stratospheric winds, but the fact that the oscillation disappears at 21.5 km and then reappears at 26.5 km implies that more than one process may be responsible. While a full analysis of the influence of the QBO on stratospheric transport and stratosphere-troposphere exchange is beyond the scope of this work, we offer some qualitative observations.

It has been proposed that the annual cycle in mean tropical tropopause height is strongly influenced by the annual cycle in extratropical wave activity, with strong wave activity during Northern Hemisphere (NH) winter resulting in a higher, colder tropopause [*Reid and Gage,* 1996]. A higher, colder tropopause would in turn result in drier air at the tropopause, which is consistent with the observation that minima in the annual cycle of $\hat{X}$ in the lowermost stratosphere occur during NH winter. Because wave activity and tropical upwelling during the QBO easterly phase are enhanced relative to the westerly phase [*O'Sullivan and Chen,* 1996], one might expect the tropical tropopause to be higher and $\hat{X}$ to be lower during QBO easterlies. The connection between QBO phase and tropopause height was demonstrated by *Reid and Gage* [1993]. We compare in Figure 3a the 50-mbar Singapore winds (available at http://nic.fb4.noaa.gov/data/cddb/) and tropical $\hat{X}_s$ at 16.5 km. As expected, $\hat{X}_s$ is lower during easterly winds ($u < 0$), and the lowest water vapor mixing ratios are observed (1990) when easterly winds occur during NH winter.

Conversely, westerly winds correspond to higher values of $\hat{X}$, with the exception of 1988–1989. Also shown in Figure 3a is the NINO4 sea surface temperature (SST) index (see section 2.). The SST in the tropical Pacific was unusually cold during the winter of 1988–1989 as a result of La Nina, and this was the only time during the 12-year period considered here that the SST dropped below the deep convection threshold of 27.5°C [*Graham and Barnett,* 1987]. The unusually low SST during the winter of 1988–1989 thus provides a possible explanation for low $\hat{X}_s$ despite the westerly QBO phase if we assume that deep convection supplies H_2O to the tropical tropopause region. We note that the relationship between SST, convection, and stratospheric humidity is further complicated by the fact that tropopause height and temperature are also affected by convection and El Nino [*Reid and Gage,* 1993]. Continued observations as the present ongoing La Nina intensifies will test our proposed link between colder SST and a drier lower stratosphere.

Because the QBO-like variations in $\hat{X}_s$ decrease with altitude up to 21.5 km (Figure 2) and then reappear at 26.5 km, we believe that the QBO may be influencing $\hat{X}$ in a different way above 21.5 km. By analyzing aerosol distributions, *Hitchman et al.* [1994] have found that the QBO modifies zonal mean transport out of the tropics and that the effects in the middle and lower stratosphere are out of phase. Similar behavior was seen in a recent modeling study [*Jones et al.,* 1998]. When there is easterly shear (descending easterlies) in the lower stratosphere, the tropical middle stratosphere is more isolated from the subtropics and vertical advection is stronger; when there is westerly shear in the lower stratosphere, the exchange between the tropics and subtropics is enhanced in the middle stratosphere and vertical advection is weaker. In a detailed study of the annual cycle in H_2O, *Mote et al.* [1996] also found that vertical advection in the tropics is enhanced when there is easterly shear.

The behavior of $\hat{X}$ is consistent with this model. We show in Figure 3b the difference between tropical and midlatitude $\hat{X}$ at 26.5 km, as well as the 50-mbar Singapore winds. The gradient between tropics and subtropics is small during periods of westerly shear (sharply increasing winds in Figure 3b), while the gradient is large and tropical $\hat{X}$ preserves the annual cycle seen at lower altitudes during periods of easterly shear (decreasing winds). The strong annual cycle at 26.5 km during periods of easterly shear reflects the increased isolation of the tropics.

6. Calculation of the Age Spectrum

We calculate age spectra using both Fourier and SVD deconvolution methods (section 2.) after substituting $\hat{X}$ for V and using $\hat{X}$ at 16.5 km in the tropics for $V(\boldsymbol{x}_0, t)$. The results are shown in Figure 4. The Fourier and SVD deconvolutions produce similar results, although the SVD method does a better job in preserving narrow features. The true tropical age spectrum at 16.5 km is a delta function at zero lag because of our definition of $V(\boldsymbol{x}_0, t)$, and the width of this feature provides an estimate of the resolution of each convolution method (≈ 0.3 year full width at

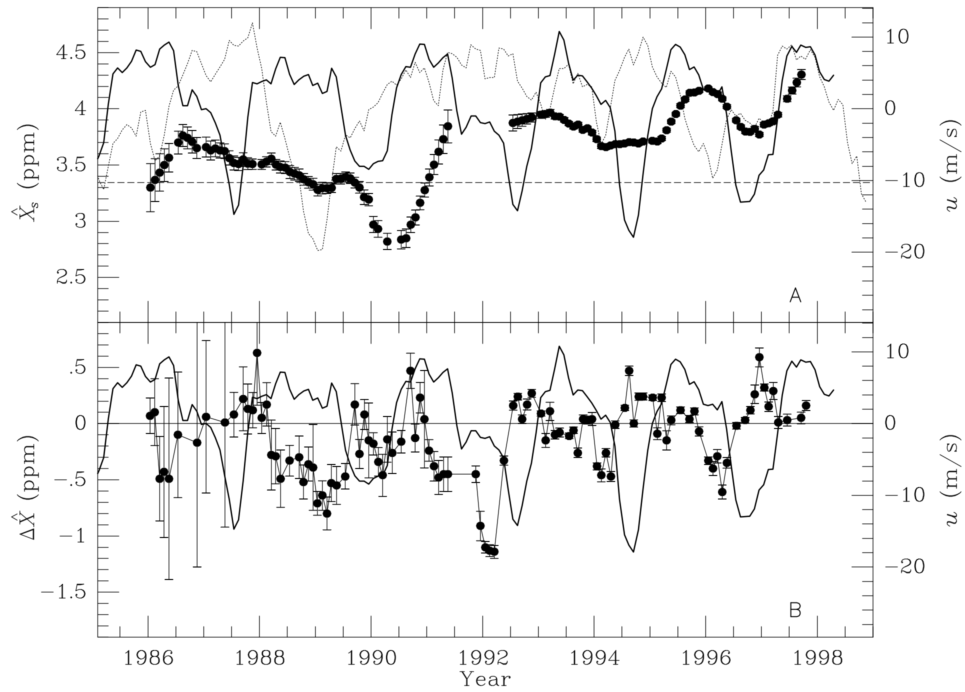

Figure 3. Comparison of $\hat{X}$ (symbols), average sea surface temperature (SST) in the region bounded by 5°N–5°S and 160°E–150°W (dotted curve), and 50-mbar Singapore winds (u, solid curve); the dashed line indicates $\mathrm{SST} = 27.5$°C. (a) Deannualized tropical $\hat{X}$ ($\hat{X}_s$) at 16.5 km. (b) The difference between tropical and midlatitude $\hat{X}$ ($\Delta\hat{X}$) at 26.5 km.

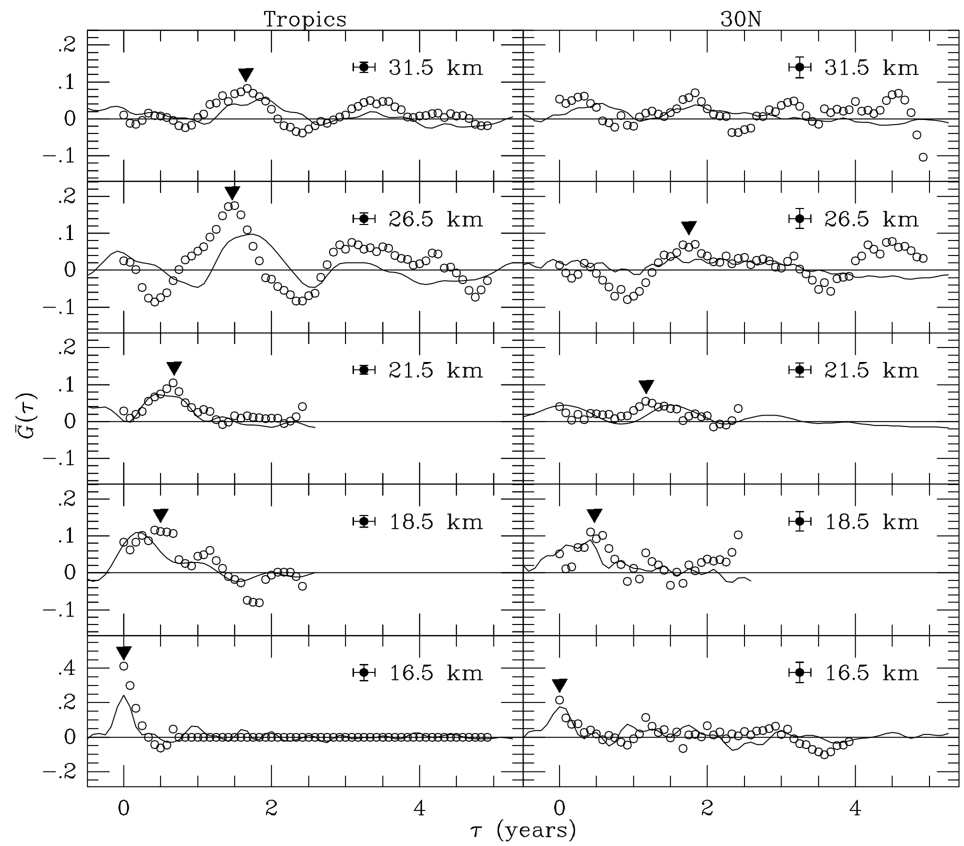

Figure 4. Calculated age spectra at selected altitudes. Fourier and SVD deconvolutions are indicated by solid curves and open circles, respectively. The calculation at 16.5 km in the tropics is included to show the time resolution after filtering; the true age spectrum would be a delta function at $\tau = 0$. Average error in $\bar{G}(\tau)$ and approximate time resolution are shown as error bars on the solid circle plotted next to each altitude legend. Estimated age spectrum peaks indicated by inverted triangles.

half maximum for the SVD method). We believe that the SVD method is superior both because it provides an error estimate and because it allows us to define $\bar{G}$ to be zero for negative lags, which is more realistic since air must pass through 16.5 km before being transported to higher altitudes.

Both methods require that we estimate missing data, although for the SVD method we require only that $V(\boldsymbol{x}_0, t)$ be defined at all lags; there is no corresponding restriction on $V(\boldsymbol{x}, t)$. All missing data are estimated using the monthly mean for the full data set at the appropriate altitude and latitude. The monthly means are also used when $t_i - \tau_j < 1986$ in (5). Extrapolating with monthly means will have the greatest effect on the (SVD) calculated age spectrum at the largest lags. We tested the effect of extrapolation by repeating the SVD deconvolution at 31.5 km without using any extrapolated data, and we found that the change in the calculated age spectrum was less than the estimated error. The lack of sensitivity of the estimated age spectrum to the use of monthly mean data, particularly in the tail at large lags, suggests that improved estimates of the age spectrum will require more observations of large-amplitude, long-period events, such as the large dip in $\hat{X}_s$ which was observed in 1990.

The true age spectrum is zero for negative lags and greater than or equal to zero for positive lags. The fact that the estimated age spectra are sometimes negative by a statistically significant amount (for example, the 26.5-km tropical result in Figure 4) suggests the presence of systematic errors. One assumption we have made which we know to be invalid is that the zonal mean age spectrum is constant in time at a given latitude. As shown in Figure 3b, the QBO produces significant interannual variability in the residual mean circulation, and variability in transport will affect the age spectrum. The fact that the tropical and midlatitude estimates of the age spectrum at 26.5 km show large (but out of phase) variations with a period between 24 and 30 months indicates that not accounting for interannual variability may be an important source of error and that averaging data over additional cycles of the QBO might reduce the effect. We note that previous modeling studies of the age spectrum have also neglected the effect of the QBO [*Hall and Waugh,* 1997, *Waugh et al.,* 1997]

The peak of the estimated age spectrum (indicated by the inverted triangles in Figure 4) can be followed up to 31.5 km in the tropics and 26.5 km at middle latitudes as it shifts to progressively greater lags. We believe that the midlatitude results at 31.5 km are not statistically significant. The peak starts at a lag of 0 years at 16.5 km in the tropics (by definition) and shifts to lags of 0.5, 0.7, 1.5, and 1.6 years at 18.5, 21.5, 26.5, and 31.5 km, respectively. At 30°N the peak also starts at 0 lag at 16.5 km and shifts to 0.5, 1.2, and 1.8 years at 18.5, 21.5, and 26.5 km, respectively. Our results are in excellent agreement with the results of the Community Climate Model, Version 2 (CCM2) presented by *Hall and Waugh* [1997], although we note that the trajectories in the CCM2 model start near the surface, not at the tropopause. We can correct for this by increasing our estimates of the age spectrum peak by the lag time of the peak at 16.5 km in the CCM2 model. While Hall and Waugh did not present results below 18 km, the lag time of the peak at 18 km was 0.2 years in the model, and this can be taken as an upper limit for the correction to the lag times given above. Moving the source from the tropopause to the surface also means that the age spectrum at the tropopause will no longer be a delta function, which will result in the modeled age spectra decaying more slowly at large lags.

We have calculated Γ directly from $\bar{G}$ using (2) and compared the results with estimates of mean age relative to the tropopause derived from in situ measurements of SF_6. Our estimates of Γ will be biased low whenever the calculation of $\bar{G}$ is not extended to sufficiently long lag times as a result of the available finite data record. Using the modeled age spectra of *Hall and Waugh* [1997] as a guide, we estimate that there is insufficient data above 21.5 km in the tropics and above 18 km at 30°N. Our estimated mean age relative to the tropopause is 0.5 ± 0.2 years at 18.5 km in the tropics and 1.2 ± 0.5 years at 16.5 km at 30°N; both estimates are in good agreement with modeling results and SF_6 measurements [*Hall and Waugh,* 1997, *Waugh et al.,* 1997].

7. Summary

We have shown that entry level H_2O is a powerful tracer of stratospheric transport. The observations suggest that humidity in the lower stratosphere is affected by the QBO through the effect of extratropical wave activity on the height of the tropical tropopause. We find that unusually low temperatures in the tropical Pacific may result in a drier lower stratosphere, a conclusion which may be confirmed or disproved by observations made through the current El Nino-La Nina cycle. We have used the observations to estimate zonal mean age spectra in the tropical and lower extratropical stratosphere, and we find that the lag time of the peak and the mean age are in good agreement with model calculations and estimates derived from observations of SF_6. While the age spectra we present here cannot produce a local, high-precision estimate of the mean age on par with in situ measurements of SF_6

or CO_2, there is additional valuable information contained in the shape of the age spectrum which cannot be derived from the mean age alone. In particular, the fact that the age spectra peak at lag times which are modest compared with the mean age estimated from SF_6 confirms that the mean age is large as a result of the age spectrum having a long tail at large lags, not because the advection timescale is long. We expect the results presented here to improve with time as the continuous record of H_2O observations provided by SAGE II and HALOE continues to grow.

Acknowledgments We gratefully acknowledge support from NASA's Upper Atmosphere Research Program in the form of grant NSG 5175. Part of this research was performed at the Jet Propulsion Laboratory, California Institute of Technology, under contract with NASA. Technical assistance for the balloon flight was provided by the Jet Propulsion Laboratory and the National Scientific Balloon Facility. We thank R. Salawitch for suggesting that we compare the trends in balloon and SAGE data. We also thank an anonymous reviewer of an earlier version of this paper for providing helpful comments.

References

Abbas, M. M., et al., The hydrogen budget of the stratosphere inferred from ATMOS measurements of H_2O and CH_4, *Geophys. Res. Lett.23,* 2405-2408, 1996.

Dlugokencky, E. J., L. P. Steele, P. M. Lang, and K. A. Masarie, The growth rate and distribution of atmospheric methane, *J. Geophys. Res.99,* 17,021-17,043, 1994.

Evans, S. J., R. Toumi, J. E. Harries, M. P. Chipperfield, and J. M. Russell III, Trends in stratospheric humidity and the sensitivity of ozone to these trends, *J. Geophys. Res.103,* 8715-8725, 1998.

Graham, N. E., and T. P. Barnett, Sea surface temperature, surface wind divergence, and convection over tropical oceans, *Science, 238,* 657-659, 1987.

Hall, T. M., and R. A. Plumb, Age as a diagnostic of stratospheric transport, *J. Geophys. Res.99,* 1059-1070, 1994.

Hall, T. M., and D. W. Waugh, Timescales for the stratospheric circulation derived from tracers, *J. Geophys. Res.102,* 8991-9001, 1997.

Harries, J. E., J. M. Russell III, A. F. Tuck, L. L. Gordley, P. Purcell, K. Stone, R. M. Bevilacqua, M. Gunson, G. Nedoluha, and W. A. Traub, Validation of measurements of water vapor from the Halogen Occultation Experiment (HALOE), *J. Geophys. Res.101,* 10,205-10,216, 1996.

Hitchman, M. H., M. McKay, and C. R. Trepte, A climatology of stratospheric aerosol, *J. Geophys. Res.99,* 20,689-20,700, 1994.

Holton, J. R., P. H. Haynes, M. E. McIntyre, A. R. Douglass, R. B. Rood, and L. Pfister, Stratosphere-troposphere exchange, *Rev. Geophys.33,* 403-439, 1995.

Johnson, D. G., K. W. Jucks, W. A. Traub, and K. V. Chance, Smithsonian stratospheric far-infrared spectrometer and data reduction system, *J. Geophys. Res.100,* 3091-3106, 1995.

Jones, D. B. A., H. R. Schneider, and M. B. McElroy, Effects of the quasi-biennial oscillation on the zonally averaged transport of tracers, *J. Geophys. Res.103,* 11,235-11,249, 1998.

McCormick, M. P., E. W. Chiou, L. R. McMaster, W. P. Chu, J. C. Larsen, D. Rind, and S. Oltmans, Annual variations of water vapor in the stratosphere and upper troposphere observed by the Stratospheric Aerosol and Gas Experiment II, *J. Geophys. Res.98,* 4867-4874, 1993.

Mote, P. W., K. H. Rosenlof, M. E. McIntyre, E. S. Carr, J. C. Gille, J. R. Holton, J. S. Kinnersley, H. C. Pumphrey, J. M. Russell III, and J. W. Waters, An atmospheric tape recorder: The imprint of tropical tropopause temperatures on stratospheric water vapor, *J. Geophys. Res.101,* 3989-4006, 1996.

Mote, P. W., T. J. Dunkerton, M. E. McIntyre, E. A. Ray, P. H. Haynes, and J. M. Russell III, Vertical velocity, vertical diffusion, and dilution by midlatitude air in the tropical lower stratosphere, *J. Geophys. Res.103,* 8651-8666, 1998.

Nedoluha, G. E., R. M. Bevilacqua, R. M. Gomez, D. E. Siskind, B. C. Hicks, J. M. Russell III, and B. J. Connor, Increases in middle atmospheric water vapor as observed by the Halogen Occultation Experiment and the ground-based Water Vapor Millimeter-wave Spectrometer from 1991 to 1997, *J. Geophys. Res.103,* 3531-3543, 1998.

Oltmans, S. J., and D. J. Hofmann, Increase in lower-stratospheric water vapour at a mid-latitude Northern Hemisphere site from 1981 to 1994, *Nature, 374,* 146-149, 1995.

O'Sullivan, D., and P. Chen, Modeling the quasi biennial oscillation's influence on isentropic tracer transport in the subtropics, *J. Geophys. Res.101,* 6811-6821, 1996.

Park, J. H., et al., Validation of Halogen Occultation Experiment CH_4 measurements from UARS, *J. Geophys. Res.101,* 10,183-10,203, 1996.

Press, W. H., S. A. Teukolsky, W. T. Vetterling, and B. P. Flannery, *Numerical Recipes in Fortran: The Art of Scientific Computing,* 2nd ed., Cambridge Univ. Press, New York, 1992.

Randel, W. J., F. Wu, J. M. Russell III, A. Roche, and J. W. Waters, Seasonal cycles and QBO variations in stratospheric CH_4 and H_2O observed in UARS HALOE data, *J. Atmos. Sci., 55,* 163-185, 1998.

Reid, G. C., and K. S. Gage, Troposphere-stratosphere coupling in the tropics: The role of El Nino and the QBO, in *The Role of the Stratosphere in Global Change*, edited by M. -L. Chanin, pp. 245-266, Springer-Verlag, New York, 1993.

Reid, G. C., and K. S. Gage, The tropical tropopause over the western Pacific: Wave driving, convection, and the annual cycle, *J. Geophys. Res.101,* 21,233-21,241, 1996.

Remsberg, E. E., P. P. Bhatt, and J. M. Russell III, Estimates of the water vapor budget of the stratosphere from UARS HALOE data, *J. Geophys. Res.101,* 6749-6766, 1996.

Rind, D., E.-W. Chiou, W. Chu, S. Oltmans, J. Lerner, J. Larsen, M. P. McCormick, and L. McMaster, Overview of the Stratospheric Aerosol and Gas Experiment II water vapor observations: Method, validation, and data characteristics, *J. Geophys. Res.98,* 4835-4856, 1993.

Russell, J. M., III, L. L. Gordley, J. H. Park, S. R. Drayson, W. D. Hesketh, R. J. Cicerone, A. F. Tuck, J. E. Frederick, J. E. Harries, and P. J. Crutzen, The Halogen Occultation Experiment, *J. Geophys. Res.98,* 10,777-10,797, 1993.

Toon, G. C., The JPL MkIV interferometer, *Opt. Photonic News, 2,* 19-21, 1991.

Toon, G. C., C. B. Farmer, P. W. Schaper, L. L. Lowes, and R. H. Norton, Composition measurements of the 1989 Arctic winter stratosphere by airborne infrared solar absorption spectroscopy, *J. Geophys. Res.97,* 7939-7961, 1992.

Waugh, D. W., et al., Three-dimensional simulations of long-lived tracers using winds from MACCM2, *J. Geophys. Res.102,* 21,493-21,513, 1997.

This preprint was prepared with the AGU LaTeX macros v3.1. File h2o˙jgr formatted 1999 July 21.